Breaking down cellulose fibrils with a mid-infrared laser

Dominik Domin, Viet Hoang Man, Nguyen-Thi Van-Oanh, Junmei Wang, Takayasu Kawasaki, Philippe Derreumaux, Phuong Nguyen

Noname manuscript No.
(will be inserted by the editor)

Breaking down cellulose fibrils with a mid-infrared laser

Dominik Domin · Viet Hoang Man · Nguyen-Thi Van-Oanh · Junmei Wang · Takayasu Kawasaki · Philippe Derreumaux Phuong H. Nguyen

Received: date / Accepted: date

Abstract A novel process for the separation of crystalline cellulose in water into single polysaccharide strands is proposed that does not require high temperatures or other chemical reactants. We have modeled the behavior of a 36-strand cellulose Iβ crystalline bundle when subjected to picosecond mid-infrared laser pulses using all-atom non-equilibrium molecular dynamics sim-

Dominik Domin*
Direction de la Recherche Fondamentale, Maison de la Simulation, USR 3441, Bâtiment 565 - Digiteo, Commissariat à l'Energie Atomique, centre de Saclay, 91191 Gif-sur-Yvette Cedex, France
E-mail: dominik.domin@cea.fr

Viet Hoang Man*
Department of Pharmaceutical Sciences, School of Pharmacy, University of Pittsburgh, Pittsburgh, PA 15213, USA

Nguyen-Thi Van-Oanh
Laboratoire de Chimie Physique, CNRS, Université Paris Sud, Université Paris-Saclay, 91405 Orsay Cedex, France E-mail: van-oanh.nguyen-thi@u-psud.fr

Junmei Wang
Department of Pharmaceutical Sciences, School of Pharmacy, University of Pittsburgh, Pittsburgh, PA 15213, USA

Takayasu Kawasaki
IR Free Electron Laser Research Center, Research Institute for Science and Technology, Organization for Research Advancement, Tokyo University of Science, 2641, Yamazaki, Noda, Chiba 278-8510, Japan

Philippe Derreumaux
Laboratoire de Biochimie Théorique, UPR 9080 CNRS, IBPC, Université Denis Diderot, Paris Sorbonne Cité, 13 rue Pierre et Marie Curie, 75005, Paris, France E-mail: derreumaux@ibpc.fr

Phuong H. Nguyen
Laboratoire de Biochimie Théorique, UPR 9080 CNRS, IBPC, Université Denis Diderot, Paris Sorbonne Cité, 13 rue Pierre et Marie Curie, 75005, Paris, France E-mail: nguyen@ibpc.fr
*Contribute equally to this work.

ulations. We show that mid-infrared laser pulses that induce resonance deformations in the C-O-H angles of the hydroxyl groups that are involved in the hydrogen bonding network of cellulose, rapidly cause the cellulose bundles to dissociate into single strands solvated by the water. The laser pulses selectively disrupt intra- and inter-chain hydrogen bonds that maintain the polysaccharide strands in sheets and bundles, causing cellulose to dissolve into single strands whose end-to-end lengths remain similar to those in the original cellulose crystalline bundle. This proof-of-concept work provides guidance for experiments that may provide insight into the mechanism of cellulase enzymes whose improvement could lead to increased production of ethanol from cellulose, and possibly spur the development of new nanomaterial engineering techniques.

Keywords: Laser; cellulose; non-equilibrium simulation; ionic liquid

1 Introduction

Cellulose is one of the most abundant biological materials on the planet, which has the potential to be transformed into biofuels that could readily replace a large fraction of petroleum-based fuels. It is estimated that by the year 2030 the United States alone could replace at least 30% of its petroleum consumption with biofuels from domestic sources[1]. Unfortunately, the molecular structure adopted by cellulose in its crystalline form makes it resistant to acid and enzymatic hydrolysis[2], a prerequisite step in the conversion of cellulose into biofuels. In fact, the pretreatment of cellulose and its cleavage into cellobiose and glucose are the most costly steps in the production of ethanol from cellulose. [3, 1]. Crystalline cellulose has its glucose monomers in the chair conformation forcing aliphatic hydrogen atoms into axial positions and hydroxyl groups in equatorial positions. The resulting linear cellulose chains form sheets with a strong hydrogen bond network between the chains and significant hydrophobic interactions between the stacked sheets.[2, 4, 5]. These two characteristic interactions contribute to the resistance of crystalline cellulose to enzymatic and acid hydrolysis[6–8]. However, amorphous and single chains of cellulose can readily be digested by enzymes into glucose that can readily be fermented into ethanol[1].

The transformation of native cellulose into glucose can be accomplished under high temperature acidic conditions or by means of an acidic pretreatment followed by enzymatic hydrolysis. While the high temperature process may be faster and less expensive than the enzymatic process, it suffers from the inconvenience of producing byproducts that poison the yeast that ferment the glucose into ethanol.[1] Enzymatic hydrolysis of cellulose is slow because crystalline cellulose is insoluble in water which reduces its mass transport properties. Furthermore, the endo-cellulase enzymes that can digest crystalline cellulose act primarily on the ends of cellulose bundles. [1] Exo-cellulase enzymes which readily act on amorphous and free strands of cellulose, are known to cooperate synergistically with endo-cellulases to hydrolyze cellulose into smaller

oligosaccharides. Mechanistic models of cellulase activity suggest that increasing the effective surface area in cellulose bundles and solubilizing cellulose strands would enhance the rate of hydrolysis of cellulose catalyzed by cellulase enzymes. [9,10] Since cellulases on their own operate one or two orders of magnitude slower than other polysaccharidases[2], one can expect a potential for improvement in enzymatic efficiency.

Cellulose can be dissolved in ionic liquids (ILs)[11,12]. However, the relatively high temperatures (most ionic liquids have melting points near 373K) and the high viscosity of ionic liquids make them less than ideal solvents for enzymatic hydrolysis of cellulose. Furthermore, the ions present in ionic liquids can cause inactivation and irreversible unfolding of cellulase enzymes.[13]

Methods have been introduced to dissolve cellulose that do not require chemical reactants. These methods include dissolution promoted by ultrasound or microwave heating. Ultrasonic energy promotes the dissolution process through its special cavitation effect. This effect generates violent shockwaves and micro-jets that can break the crystalline cellulose into individual chains, and therefore enhances the hydrolysis[14]. However, the exact mechanism of ultrasonic intensification is still unclear and needs to be further studied.

Microwave heating has been successfully applied to dissolving cellulose[11]. Since microwave energy can in principle easily penetrate inside cellulose bundles, the whole system could be heated simultaneously and thus making it more uniform and efficient than conventional boiling. While microwave heating may solve the heat transfer resistant problem, microwave energy is strongly absorbed by water or ionic liquids and thus very little of the energy is actually transferred directly to cellulose. Furthermore microwave heating occurs rapidly which can easily lead to degradation of the ionic liquid solvents and cellulose, or even explosions of studied systems. For excellent reviews of these methods, readers are referred to recent publications[15–17].

In this article, an alternative method using laser pulses for dissolving cellulose in water is explored computationally. Indeed, this idea has been previously developed and experimentally applied to dissociate protein self-assembled nano structures[18–22]. In this simulation study, the mechanism and dynamics of the laser induced dissociation of the cellulose bundle and the subsequent solvation are explored. A 36-strand cellulose bundle models the recalcitrant crystalline core of a plant cell wall microfibril. The cellulose bundle is subject to mid-infrared laser pulses that are in resonance with the hydroxyl vibrational angle bending modes. This rapidly leads to the dissolution of the cellulose in water. Our proposed dissociation method is fast, simple, and with a well-defined mechanism. It can be used to dissolve cellulose directly in water or in combination with ionic liquid solvent, and may open new and efficient ways for dissolving cellulose.

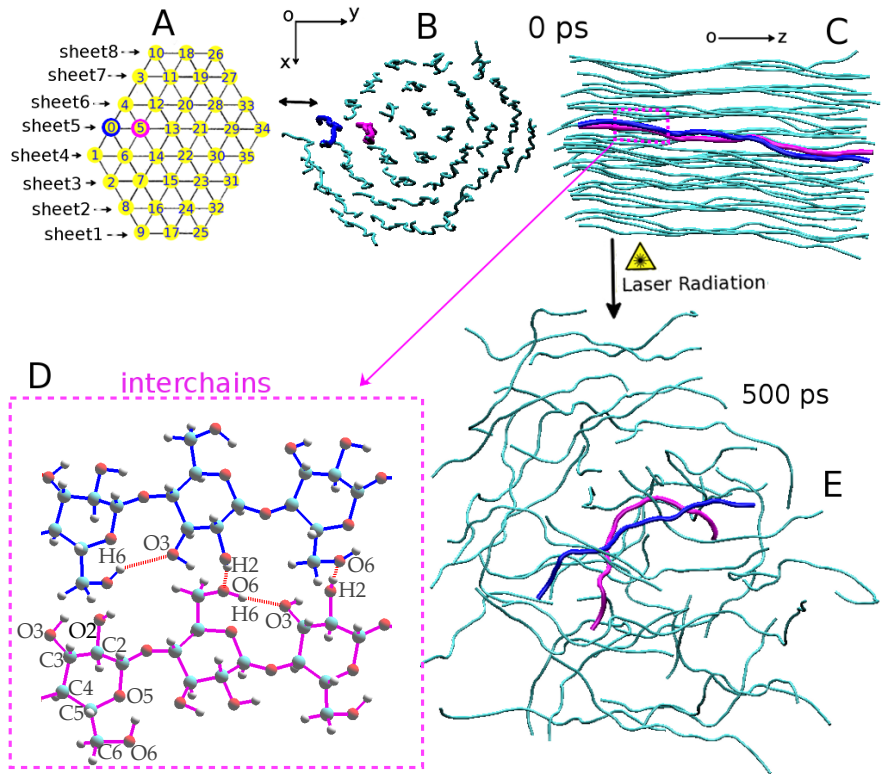

Fig. 1 (A) Labeling of the 36-chain cellulose Iβ microfibril model. Each chain has 12 glucose residues. The view along the drection parallel and perpendicular to chains are shown in (B) and (C), respectively. (D) Close-up view of two selected chains to show the intra-chain O6H6$\cdots$O3, hydrogen bonds and the inter-chain O2H2$\cdots$O6 hydrogen bonds. (E) A snapshot obtained after 500 ps laser excitation with the laser frequency $\omega_L = 1360$ cm^{-1} and intensity $E_0 = 2$ Vnm^{-1}.

2 System and methodology

2.1 System preparation

In this work, we employ the cellulose-builder program[23] to build a 36-chain cellulose Iβ model, each chain consists of 12 β D-glucose residues. While 18-24 chain cellulose elementary fibril models have also been recently proposed [24], models with 36 chains and large degree of polymerization are thought to model reasonably well the recalcitrant crystalline core of a plant cell wall microfiber[25] and are often used as a representative model for computational studies [26–36]. In this model, chains are alligned parallel to form sheets and the sheets are stacked together as shown in Figs.1(A),(B),(C). The structure is then solvated in an octahedral simulation cell containing 24237 water molecules, resulting in 81891 atoms in total.

Matthews and colleagues have compared hydrated equilibrium structures of the 36-chain cellulose Iβ microfibril using three force fields CHARMM35, GLYCAM06 and GROMOS 445a4. They found that CHARMM35 and GLYCAM06 result in structures similar to those observed in experiments, but GROMOS 45a4 leads to differences[34]. Given those results, we decided to use the CHARMM C36 force field[37,38] to model cellulose and the TIP3P water model[39] to describe the solvent.

Starting from our constructed cellulose bundle system, a short simulation of 1 ns was carried out in the constant pressure ($P = 1$ bar) and constant temperature ($T = 300$ K) ensemble (NPT) followed by 500 ns of equilibration constant volume and constant temperature (NVT) simulations at 300 K, employing the GROMACS program.[40] All bond lengths containing hydrogen atoms were constrained using the SHAKE algorithm[41] and the equations of motion are integrated with a time step of 2 fs using a leapfrog algorithm. The electrostatic interactions were calculated using the particle mesh Ewald method with a cutoff of 1.1 nm [42]. A cutoff of 1.2 nm was used in the evaluation of Van der Waals interactions. The nonbonded pair lists were updated every 10 fs. Temperature was controlled by the Berendsen thermostat[43] with a coupling constant of 0.1 ps. One hundred statistically independent equilibrium conformations were selected from the last 100 ns of the NVT trajectory and subsequently used for IR spectrum calculations and the laser-induced non-equilibrium molecular dynamics (NEMD) simulations.

2.2 IR spectrum calculations

For the selected conformations, the thermostat was turned off and subsequent 1 ns constant volume and constant energy (NVE) simulations were performed with a time step of 0.5 fs. This smaller time step was chosen to properly describe the vibrational motions. Dipole moments $\boldsymbol{\mu}(t)$ were saved every 1 fs, and the IR spectrum of the cellulose solvated in water was then calculated directly using the Fourier transformation of the classical time autocorrelation of the dipole moments. Due to the use of the classical autocorrelation function, the double harmonic quantum correction protocol we previously developed [44] was applied to correct the IR intensities. Thus, the IR spectrum, $\mathcal{I}(\omega)$, is obtained using the following expression:

$$\mathcal{I}(\omega) = \frac{2\pi\omega^2}{3c\,V\,k_B T} \int_{-\infty}^{\infty} \exp(-i\omega t)\langle \boldsymbol{\mu}(0).\boldsymbol{\mu}(t)\rangle dt. \tag{1}$$

where ω is the frequency, k_B is the Boltzmann constant, c is the speed of light, and V is the volume. The expression $\langle \boldsymbol{\mu}(0).\boldsymbol{\mu}(t)\rangle$ represents a statistical average of the correlation of the dipole moment over the 1 ns NVE trajectories.

Assigning the vibrational modes of the cellulose based on direct Hessian calculations is unfortunately not tractable due to the large size of the system. In order to remedy this problem, for the assignment of vibrational modes, the

power spectrum of selected atoms was calculated using the time autocorrelation of their velocities.

2.3 Laser-induced simulation

The NEMD method has been developed and successfully applied to study various systems including amyloid fibrils[45], peptide nanostructures[46], DNA duplex[47] and viruses[48], it is useful to briefly summarize the main aspects of the method here. During the NEMD simulations, a time-dependent electric field

$$E(t) = E_0 \exp[-\frac{(t-t_0)^2}{2\sigma^2}] \cos[2\pi c\omega_L(t-t_0)], \quad (2)$$

was applied to mimic a laser micro-pulse [Fig.2](A)]. Here, E_0 represents the amplitude of the electric field, σ is the pulse width, t is the time, t_0 is the time where the pulse has maximum amplitude, and ω_L is the laser frequency. In our NEMD simulations, only the water molecules are coupled to the thermostat in order to maintain the temperature of 300 K. Finally, to ensure stability, a time step of 0.2 fs was used, and data was collected every 0.1 ps.

3 Results and Discussions

3.1 IR spectrum and hydrogen bond network of the cellulose

Cellulose Iβ has three important regions of absorption in the IR spectrum: 950-1200 cm^{-1} which involves C-O stretches, 1250-1450 cm^{-1} which corresponds to C-O-H and C-H bending motions, and 3200-3500 cm^{-1} which corresponds to O-H stretches.[49–54] We focus only on the frequencies of the C-O-H bending region since it does not overlap with frequencies present in the IR spectrum of water, in particular, the OH bending and OH stretching modes that are located at 1645 cm^{-1} and 3404 cm^{-1}, respectively[55,56]. We also avoid exciting vibrational modes in cellulose (such as the C-O stretch) that are not directly involved in the hydrogen bond network that keeps cellulose bundles intact. We avoid exciting any vibrational frequencies present in water in order to control the dissociation of cellulose hydrogen bonds rather than simply heating up the water solution. Our calculated IR spectrum of the cellulose in water in this mid-IR frequency region is shown in Fig.2(B). One sees that the spectrum displays two intense bands at 1274 cm^{-1} (peak full width at half maximum, FWHM, of 63 cm^{-1}) and at 1360 cm^{-1} (FWHM = 61 cm^{-1}). In order to assign these peaks, the power spectra of the C2-O2-H2, C3-O3-H3 and C6-O6-H6 hydroxyl angles, which are involved in the formation of intra- and inter-chain hydrogen bonds, were calculated. Based on this analysis, the peak at 1274 cm^{-1} is assigned without ambiguity to the C2-O2-H2 bending angles. At ω = 1360 cm^{-1}, we found that all these three angles contribute to the band but the dominant contribution comes from the C3-O3-H3 angles

and a small contribution from the C6-O6-H6 angles. Thus, the band at 1360 cm^{-1} is assigned primarily to the deformation of the C3-O3-H3 angles. In the region of interest, a published experimental spectrum [52] of crystalline cellulose places a peak at 1281 cm^{-1} and three peaks (1338, 1354, and 1371 cm^{-1}) that merge into one broad peak with an estimated FWHM of about 50cm^{-1}. Tsuboi *et al.*[49] and Higgins *et al.*[50] assigned the bands at 1335 cm^{-1} and 1450 cm^{-1} and possibly the bands at 1205 and 1232 cm^{-1} to the OH in plane deformations. Nevertheless, Nelson and coworkers [53] confirmed later that the band at 1335 cm^{-1} and possibly the band at 1225 cm^{-1} are assigned to the OH in-plane bending motions. The frequencies of C-O-H bending modes obtained by the CHARMM36 force field are overestimated by 25 and 50 cm^{-1} for the band at 1335 cm^{-1} and at 1225 cm^{-1}, respectively. Hence our mid IR spectrum is in reasonably good agreement with these experimental spectra and with other theoretical spectrum using the GLYCAM06 force field[57] in terms of both peak positions and mode assignments.

There are two types of intra-chain hydrogen bonds in crystalline cellulose Iβ: O3H3$\cdots$O5 and O2H2$\cdots$O6. There is one type of inter-chain hydrogen bond: O6H6$\cdots$O3. Due to the small size of our 36-chain cellulose model it has a large surface area to volume ratio that once placed in water causes the geometry to slightly deform relative to the crystalline geometry. The presence of water modifies the intra-chain hydrogen bonds at the surface with the H3 hydrogens no longer pointing towards O5 oxygens, unlike in the core of the cellulose bundle, but rather towards the O2 oxygens, creating a new type of intra-chain hydrogen bonds. At the surface of the solvated cellulose bundles the inter-chain O6H6 $\cdots$O3 hydrogen bonds become intra-chain hydrogen bonds and the intra-chain O2H2$\cdots$O6 hydrogen bonds are now inter-chain hydrogen bonds. The chains in the core of our cellulose bundle have the normal hydrogen bonds deduced from experimental crystallographic studies of cellulose Iβ. In our solvated cellulose model there are 325 intra-chain and 148 inter-chain hydrogen bonds. The intra-chain hydrogen bond between O6H6$\cdots$O3 is the most dominant one (154) which represents a third of the total number of hydrogen bonds. The second most dominant intra-chain hydrogen bond is between O3H3$\cdots$O2 (93) which accounts for 20%. Strong inter-chain hydrogen bonds between O2H2$\cdots$O6 (48) and weak inter-chain CH$\cdots$O hydrogen bonds between sheets (50), each represent roughly 11% of the total number of hydrogen bonds.

3.2 Resonance between the cellulose and laser field

Our working assumption of the laser-induced dissolution method is that resonance between the infrared laser field [Fig.2(A)] and vibrational modes of the cellulose can directly induce the dissociation of cellulose bundles. As shown above, we have identified two dominant vibrational modes in the mid-IR region having frequencies of 1274 cm^{-1} and 1360 cm^{-1} [Fig.2(B)]. To see whether the resonance induced dissociation takes place if the laser targets these two modes,

we scan 100 laser frequencies [ω_L in Eq. 2] in the interval of $\omega_L = 1250 - 1450$ cm^{-1} with a spacing of 2 cm^{-1} between frequencies. For each frequency we carry out 20 NEMD simulations, each lasting 20 ps, starting from the above selected equilibrium conformations. Each conformation is run with 100 different values of ω_L, thus we have in total 2000 trajectories. Due to the large number of simulations and since we only aim to obtain the response of the cellulose, it is sufficient to use only one laser pulse [Fig.2(A)] with an intensity, E_0, of 2 Vnm^{-1}.

We calculate the maximum value of the C2-O2-H2, C3-O3-H3 and C6-O6-H6 angle fluctuations upon the laser irradition on the cellulose. For each angle, the angle fluctuation is defined as

$$< \Delta\alpha(t) >= \frac{1}{4320} \sum_{i=1}^{432} \sum_{j=1}^{10} |\alpha_i^j(t) - \alpha_{\rm eq}|, \tag{3}$$

where $\alpha_i^j(t)$ is the time evolution of the i-th angle of the j-th trajectory, and $\alpha_{\rm eq}$ is its equilibrium value (which are 102.8°, 102.3° and 106.0° for C2-O2-H2, C3-O3-H3 and C6-O6-H6 angles, respectively). Note that our model cellulose bundle consists of 36 chains of 12 glucosides thus there are 432 angles in total. These angle fluctuations are calculated at two specific times: at 10 ps when the laser pulse intensity is maximum and at 20 ps when the pulse has vanished. We also calculate at 20 ps the ensemble averages of various structural quantities including the total number of intra-chain O6H6$\cdots$O3 and O3H3$\cdots$O2 hydrogen bonds, the inter-chain O2H2$\cdots$O6 hydrogen bonds, and the root-mean-squared deviations (RMSD) of the whole cellulose with respect to the initial structure. These values are plotted against the scanned frequencies in Fig.2.

As can be seen in Fig. 2(C), when the laser intensity is maximal at 10 ps, the largest change ($\sim 9°$) is observed in the fluctuation of the C3-O3-H3 angles at $\omega_L = 1360 \pm 2$ cm^{-1}. The other two angles C2-O2-H2 and C6-O6-H6 are hardly affected. However, due to the anharmonic coupling between the angles, the primary excitation of the C3-O3-H3 angle bending motion at 1360 cm^{-1} induces the excitations of the C6-O6-H6 and C2-O2-H2 counterparts at 20 ps [Fig.2(D)] through the energy transfer along the intra- and inter-chain hydrogen bonds. This process leads to the dissociation of the whole structure as can clearly be seen from a snapshot of the configuration shown in Fig.1(E) after 500 ps. More quantitatively, the dissociation is reflected by the significant decrease in the total number of the intra-chain hydrogen bonds O6H6$\cdots$O3 ($\sim$ 45%), O3H3$\cdots$O2 ($\sim$ 65%) and inter-chain hydrogen bonds O2H2$\cdots$O6 ($\sim$ 30%) as compared to their initial equilibrium values [Fig.2(E)]. As a consequence, the chains separate as is reflected in the increased RMSD of the cellulose bundle from $\sim$ 1 Å to $\sim$ 1.3 Å [Figs.2(F)]. Finally, we note that the laser excitation at $\omega_L = 1274$ cm^{-1} also causes a resonance with the C2-O2-H2 angle bending vibration, but since its absorption cross-section is lower than that at $\omega = 1360$ cm^{-1}, only weak dissociation is observed as seen from the weak response of the angle fluctuations as well as the structural

quantities at this frequency. In summary, there is indeed a strong resonance between the laser field with the C3-O3-H3 angle bending vibrational mode at the frequency of $\omega = 1360$ cm^{-1}, confirming our working assumption. Since this laser excitation frequency is far from the stretching and angle bending frequencies of the water, it is safe to assume that water is not directly heated by the laser, and that the use of a rigid water model such as TIP4P[58], SPC[59] or TIP3P used in our simulation should not affect the results of our simulations.

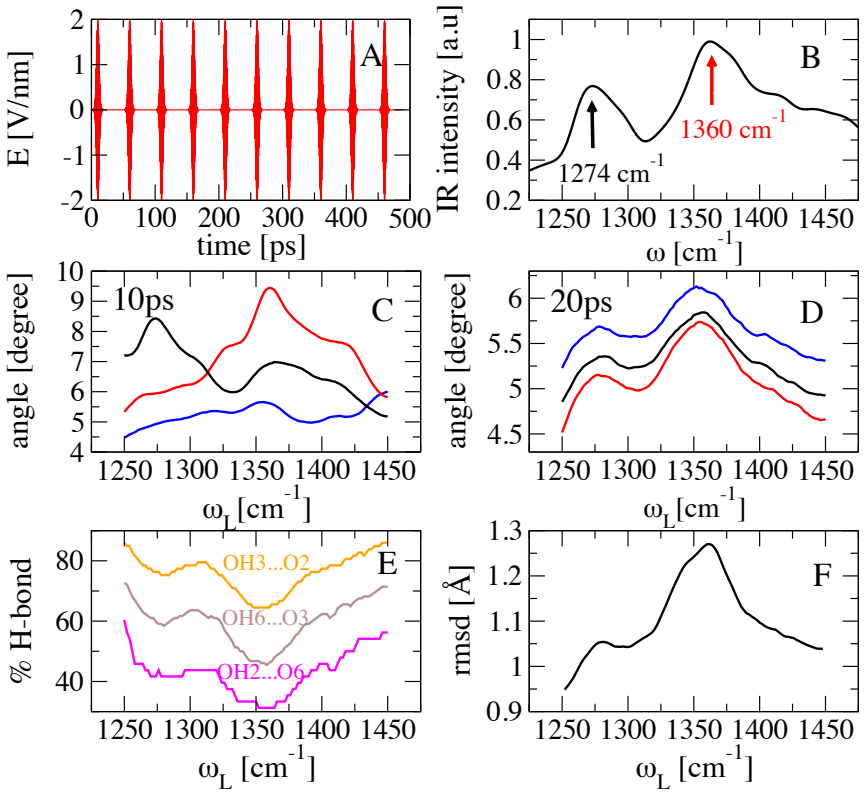

Fig. 2 (A) 10 laser pulses with $\omega_L = 1360$ cm^{-1}, E_0=2 Vnm^{-1}, $\sigma = 2$ ps, $t_0 = 10$ ps and the interval between pulses is 50 ps; (B) the IR spectrum of the cellulose in the mid-IR region; The laser-induce changes in various structural quantities as a function of the laser frequency including: (C and D) fluctuations of the angles C2-O2-H2 (black), C3-O3-H3 (red) and C6-O6-H6 (blue) at 10 ps and at 20 ps, respectively; (E) the percentage of the remaining intra-chain O6H6$\cdots$O3 (brown), O3H3$\cdots$O2 (orange) and inter-chain O2H2$\cdots$O6 (magenta) hydrogen bonds; (F) the RMSD with respect to the initial structure. A single laser pulse was used in (C) through (F).

3.3 Laser-induced cellulose dissolution process

We present now the results of the dissolution process that follows the excitation at this frequency. Starting from selected equilibrium MD conformations, we carry out NEMD simulations, each lasting 500 ps. During this time, 10 micro-pulses with parameters ($\sigma = 2$ ps, $t_0 = 10$ ps, $\omega_L = 1360$ cm^{-1}, $E_0 = 2$ V nm^{-1}) separated by a time interval of 50 ps are applied to the system. As

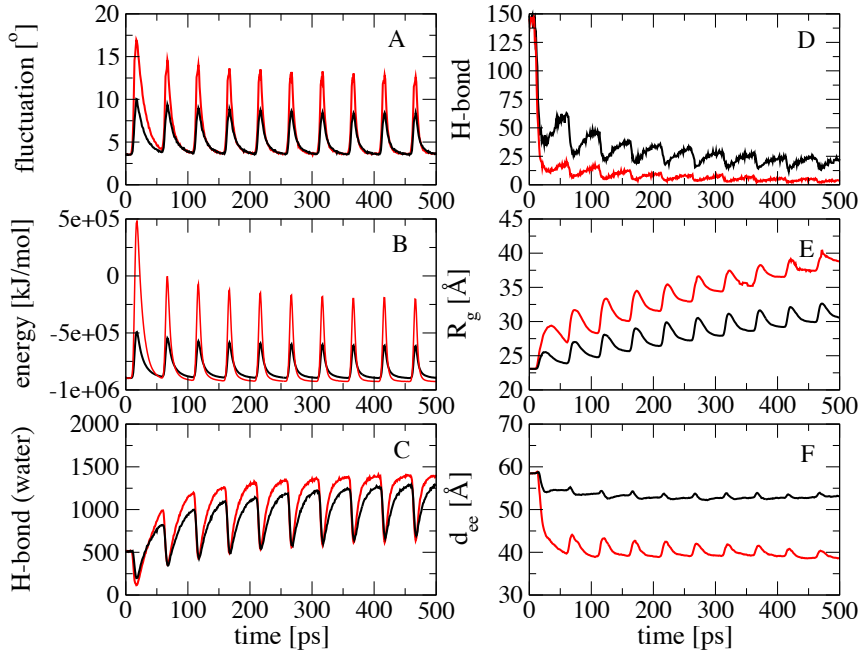

Fig. 3 Time evolution in (A) the fluctuations of the C3-O3-H3 angles; (B) the total energy of the system; (C) the number of hydrogen bonds between cellulose and water; (D) the number of the inter-chain hydrogen bonds in cellulose; (E) the radius of gyration; (F) the end-to-end distances of individual chains. Shown are results obtained from the NEMD simulation using 10 micro-pulses with $\omega_L = 1360$ cm^{-1}, $E_0 = 2$ Vnm^{-1} (black) or $E_0 = 4$ Vnm^{-1} (red).

can be seen in Fig.3, upon the irradiation with the first laser pulse, resonance occurs immediately and the C3-O3-H3 angle bending vibrational mode is excited. This results in large fluctuations of these angles with the maximal value of $\sim 9°$ around 10 ps, which represents the peak of the laser pulse [Fig.3(A)]. The excess angle bending potential energy induced by the laser pulse is then converted into kinetic energy, resulting in the increase of the total energy of the system [Fig.3(B)]. This leads to two consequences. First, the local heating of the cellulose scatters surrounding waters away from the cellulose, generating an empty space which could be considered a bubble. Thus, the number of hydrogen bonds between the cellulose and surrounding waters decreases from the

initial value of $\sim$ 500 down to $\sim$ 200 [Fig.3(C)]. Second, the strong fluctuations in the C-O-H angles that involved inter-chain hydrogen bonds are excited and broken which quickly reduced from the initial values of $\sim$ 150 down to $\sim$ 40 within the first 20 ps [Fig.3(D)]. These two effects lead to the destabilization and eventually dissolution of cellulose as indicated by an increase in the radius of gyration from $\sim$ 22 to 26 Å [Fig.3(E)]. While the cellulose chains separate as indicated by the large reduction in the number of the inter-chain hydrogen bonds, the end-to-end distance of the chains undergoes only relatively small changes from the initial value of 58 to 55 Å [Fig.3(E)]. This indicates that the laser excitation targets precisely the hydroxyl groups, which is sufficient to dissociate the cellulose into individual chains whose initial linear structure is largely maintained during the initial resolvation. After 10 ps of the first pulse, the laser intensity decreases, the fluctuation of the C3-O3-H3 angles becomes smaller and the cellulose is cooled down to the initial energy [Figs.3(A),(B)]. As a consequence, the surrounding waters get closer and form more hydrogen bonds with the cellulose as indicated by the increase shown in Fig.3(C). It is notable that the number of hydrogen bonds ($\sim$ 817) at the end of the first pulse (50 ps) is higher than the initial number of hydrogen bonds ($\sim$ 500) which can be explained by the separation of the cellulose chains leaving more space for waters to re-enter the interior of the cellulose bundle and thus forming more hydrogen bonds than were possible in the original cellulose bundle. The increase in the inter-chain hydrogen bonds and decrease in the radius of gyration can be seen in Figs.3(D) and (E). To understand this tendency for the reassembly of the cellulose chains, we analyzed the inter-chain Coulombic and Van der Waals interactions of the cellulose. We found that these two interactions are comparable, with $\approx 55 \times 10^6$ kJ/mol for the Coulombic energy and $\approx 7 \times 10^6$ kJ/mol for the Van der Waals energy. This indicates that both interactions play an important role in the stabilization of the cellulose. This also indicates that although the hydrogen bond network is broken during the exposure to the laser pulse, the Van der Waals interactions force the system to condense back closely to the agreggate structure at the end of the laser pulse. Finally, the end-to-end distance of the chains does not show a large contraction after the first pulse, indicating that the laser excitation does not substantially affect the intramolecular conformations of the chains. After 50 ps, the laser is turned on again and the second pulse excites the system one more time leading to further destabilization. This process is periodically repeated over 500 ps. Although the structure after 500 ps appears to be largely dissolved, its overall linear shape is essentially maintained [Figs.1,3(F)]. This implies that the laser excitation may indeed an ideal method for dissociation of cellulose without damaging individual chains.

This work and our previous works[45–48] show that the dissociation mechanism requires the resonance between the laser field and vibrational modes of the system. It well known from fundamental physics that the resonance condition depends largely on the specific frequency rather than the intensity of the external force. Therefore, we focused on the determination of the laser frequency that is resonant with vibrational modes of cellulose that lead to its

dissociation. In our simulations this frequency, $\omega_L = 1360$ cm^{-1}, was used and the laser intensity E_0 was varied until cellulose dissolved within a reasonable simulation timescale of 500 ps. As demonstrated with $E_0 = 2$ and 4 Vnm^{-1}, the laser intensity does not affect the dissolution mechanism, but rather only accelerates or slows down the process. In the mid-IR FEL experiments performed by Kawasaki and coworkers for dissociation of amyloid fibrils[60–63] , the laser intensity is much weaker but the irradiation duration is much longer.

While our repetition rate of 50 ps is shorter than the mid-IR FEL experimental value of 350 ps, as can be seen in Fig.3(B), the system energy tends to be equilibrated after 50 ps. Thus this timescale is sufficient to avoid the excessive overheating of cellulose, while allowing us to excite the system several times within the 500 ps simulation run. Experimental continuous mid-IR lasers on the other hand could mimic the short duration between laser pulses and could potentially be used for dissolving cellulose.

Analyzing the behavior of structural and energetic properties during the transformation of the crystalline Iβ cellulose to amorphous cellulose can give insights into the laser excitation process. As seen in Fig.3, right after the 3rd laser pulse (around 100 ps), inter-chain hydrogen bonds are no longer formed and the initial crystalline structure of the cellulose is deformed. From the 8th to 10th laser pulse ($\approx$ 400-500 ps), the increasing number of hydrogen bonds between the cellulose and water indicates that water has already entered inside the cellulose bundle. Nonetheless, additional laser excitations at 1360 cm^{-1} (C3-O3-H3 bending mode in cellulose Iβ) continue to induce similar angle fluctuations ($\approx 9°$) and the same amount of energy is absorbed by the cellulose with each pulse. This indicates that the frequency of C-O-H bending modes does not depend on the shape of the cellulose (crystalline or amorphous), unlike the high frequency of O-H stretching modes which are significantly shifted with different cellulose lattice types and different intra- and inter-molecular hydrogen bonding arrangements[49,64,51,65]. This results is not surprising in the sense that the O-H bending modes tend to be more rigid than O-H stretching modes, which is consistent with the experimental data showing that OH bending modes appeared to be less affected by their surrounding environment[49,64,53,54,56].This striking feature is helpful in the design of laser excitation experiments: one can continue to deposit energy into cellulose strands by exciting the same C-O-H bending frequency even after the cellulose is completely dissociated.

3.4 Comparison with ionic liquid dissolution process

As previously mentioned, ILs are currently the most widely used method for dissolution of cellulose while keeping the individual chains intact. Experimentally it has been shown that both the cation and anion of ILs influence the dissolution of cellulose. While the role of the anion seems to be clear, and the solubility trends follow the anion's basicity, the role of the cation is less clear. Some studies have concluded that cations hydrogen bond to cellulose, while

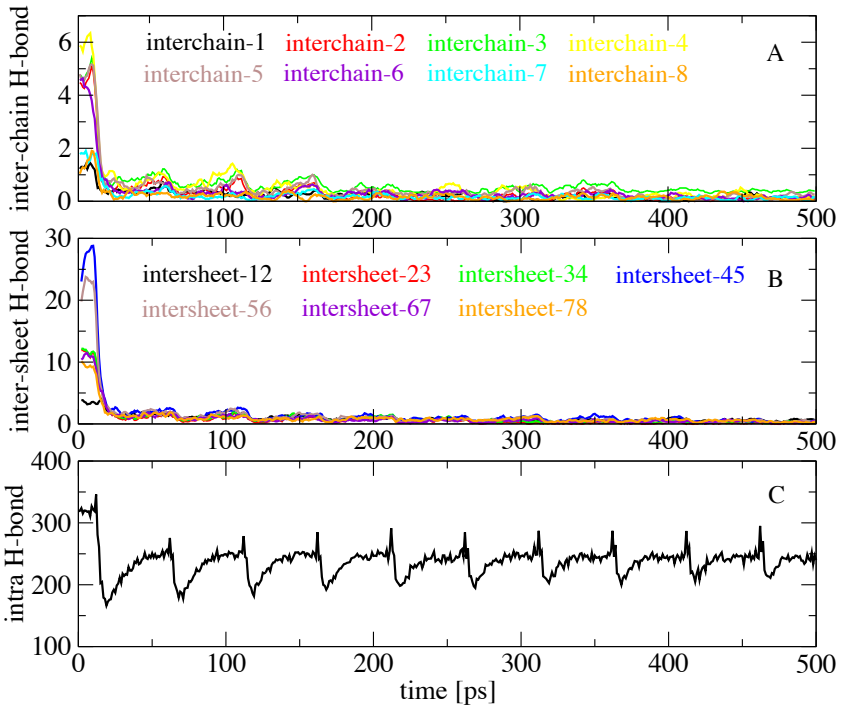

Fig. 4 Time evolution of the strong inter-chain O2H2$\cdots$O6 hydrogen bonds within a sheet i (A), weak inter-sheet CH$\cdots$O hydrogen bonds between sheets i and j (B), and the total number of intra-chain O6H6$\cdots$O3 and O3H3$\cdots$O2 hydrogen bonds of cellulose (C). The index of sheets and chains are shown in Fig.1(A). Shown are results obtained from the NEMD simulation using 10 micro-pulses with $\omega_L = 1360$ cm^{-1} and $E_0 = 2$ Vnm^{-1}.

others suggest they are not[16]. From the theoretical side, a number of MD simulations have been performed under equilibrium conditions to understand the dissolution mechanism induced by ILs[66,67]. The main finding was that anions strongly bind to the hydroxyl groups of chains on the surface of the bundle, forming negatively charged complexes. Cations then enter between the individual chains, likely due to charge imbalances, pushing the chains apart and initiating the separation. This leads to the detachment chain by chain from the main bundle in discrete rapid events. As shown in Fig.4(A), upon exposure to the laser, the inter-chain hydrogen bonds within sheets including those at the surfaces (sheets 1 and 8) and those in the interior are destroyed simultaneously due to the resonance of the bending mode with the laser. In this context, the laser-induced dissolution process should be faster than that induced by ILs. Concerning the interactions that are responsible for the dissolution of cellulose, the simulation of Cho and colleagues has shown that it is necessary to break both inter-chain and inter-sheet hydrogen bonds to dissolve cellulose,[67] and disrupting inter-chain hydrogen bonds alone is not

sufficient for explaining IL's ability to dissolve cellulose[68]. When properly tuned our laser to target precisely the hydroxyl groups for the breaking of the intra- and inter-chain hydrogen bonds network to dissolve cellulose as seen in Fig.2(E). This demonstrates the efficiency of our method for the dissolution of cellulose. Finally, the simulations of Ismail and colleagues for celluloses Iα and Iβ in three different ILs have shown that the breakage of intra-chain hydrogen bonds is necessary for reducing the rigidity of individual chains, which in turn facilities the detachment of the chains[66]. As shown in Fig.4(C), a third of the intra-chain hydrogen bonds are broken and the reduction in the number of intra-chain hydrogen bonds from the initial value of 325 to 242 after 500 ps is sufficient to destroy the inter-sheet hydrogen bonds as shown in Fig.4(C). Since two thirds of the intra-chain hydrogen bonds remain the chains are separated but their intramolecular linear structure can be largely maintained. Consequently, the large surface area of the linear cellulose chains would enhance the rate of cellulase catalyzed hydrolysis of cellulose[9,10].

4 Conclusions and Perspectives

In prior studies, Kawasaki and colleagues have studied using mid-IR free-electron lasers (FEL) to dissociate pathogenic amyloid fibrils into their monomeric forms[60–63]. Recently we have developed a comprehensive laser-induced NEMD simulation method and applied it to the dissociation of various systems including amyloid fibrils[45], peptide nanostructures[46], DNA duplex[47] and viruses[48]. Both the experiments and the theoretical studies relied on the resonance between the laser field and the amide I band 1620 - 1680 cm^{-1} (C=O bond stretching mode) of proteins. In this work, we simulated the use of a high intensity mid-IR laser to dissolve cellulose. Our laser-induced NEMD simulations show that by tuning the laser frequency precisely to that of the C3-O3-H3 angle bending vibrational mode (1360 cm^{-1}) in β D-glucoses, the excited cellulose bundle breaks its intra- and inter-chain hydrogen bonds which subsequently leads to the dissociation of the cellulose bundle. Since there are no vibrational modes of water in the region of 1360 cm^{-1}, only cellulose is directly excited. In this context, the dissolution of cellulose is simpler than that of protein-based systems because the targeted amide I band is ubiquitous in proteins and also overlaps with the bending mode of water, thus not only the targeted system will be excite but so will water and other surrounding proteins. These excitations could lead to severe damage to the surroundings and thus limit the usefulness of the technique if it is applied *in vivo*.

Although we only focused on cellulose Iβ in this work, it is worth mentioning that there are least three other crystalline cellulose structures: Iα, II and III. Cellulose II is the most common cellulose formed after industrial mercerization (alkali treatment) and regeneration (solubilization and subsequent recrystallization). Unlike the celluloses Iα and Iβ which have only hydrogen bonding network in sheets, cellulose II possesses both intra-sheet and inter-sheet hydrogen bondings.[69,70] Cellulose III can be formed from mercerized

celluloses by liquid ammonia.[71] The crystalline structure of cellulose III is similar to cellulose II and it is mainly stabilized by a large number of inter-sheet hydrogen bondings that are entirely missing in cellulose I.[72] The main purpose of this work is simulate conversion of the most stable crystalline polymorph, cellulose Iβ, into amorphous cellulose so that it can be digested by cellulase enzymes. The hydrolysis rates of cellulose II and III are approximately three times higher than that of untreated cellulose.[73,74,72] Therefore, we did not perform simulations on cellulose II and III since they are known to be more readily digested by cellulase enzymes. The other crystalline cellulose polymorphs also have C-O-H bending modes that are coupled to inter-sheet hydrogen bonds and similar computational studies could be performed to excite the C-O-H bending modes by laser pulses tuned to be in resonance with those particular frequencies. We examined the experimental infrared spectra of the different crystal lattice types of cellulose available in the literature to see how the C-O-H bending mode changes with the crystallinity. Nelson and coworkers compared the infrared spectra (in the 850-1500 cm^{-1} region) of highly crystalline samples of cellulose containing the lattice types I, II and III.[53,54] They found that the region between 1200 and 1400 contained several bands, of which the band at 1335 cm^{-1} (which corresponds to the C-O-H bending mode) appeared conserved by the different lattice types. One could conclude that hydrogen bonding does not induce any notable red or blue shifts on the frequency of the C-O-H bending modes. Regarding the intensities of the C-O-H bending modes, they observed that the intensity of this band in celluloses I, II and III is similar. Hence from the experimental results, we can assume that the laser can be operated at the same frequency for celluloses II and III as for cellulose Iβ, possibly only needing to modulate the duration of the laser irradiation.

From our simulations using the CHARMM36 force field, we were able to assign the band at 1360 cm^{-1} in our spectrum to the C3-O3-H3 bending mode, which would be difficult to attribute experimentally since the C-O-H bending modes are insensitivity to hydrogen bonding. The only noteworthy feature is the change in polarization of this band in going from cellulose I to cellulose II[64]. The attribution at 1360 cm^{-1} to C3-O3-H3 bending mode may be dependent on the type of force fields used in the simulations. We are currently planning to perform higher level simulations using a more accurate quantum electronic description of the cellulose such as density functional theory and density functional based tight binding methods to address this question.

Although we only studied a 36-strand cellulose crystalline bundle the dissociation mechanism is expected to be the same for larger cellulose bundles, since dissociation is locally initiated by the breakage of hydrogen bonds between neighboring cellulose chains. From the technical side, due to large system sizes of cellulose fibrils, current equilibrium all-atom MD simulations are limited to exploring details on small scales involving the local hydrogen bond network, water arrangement at the fibril surface, interactions between cellulose layers within the fibril, temperature dependence, effect of solvents and so forth[75, 29,67,66,26–29,31–36]. Recently, several coarse-grained force fields have been

developed for cellulose,[76–79] which would increase the size of the systems that can be studied and the simulation time-scales that are accessible. As shown above, our all-atom NEMD simulation method can induce conformational changes within picosecond timescales, thus its application to very large cellulose fibers is quite feasible, thus can provide a valuable method in addition to the current approaches to further elucidating other structural aspects of cellulose at the atomistic level.

Finally, the mid-IR laser induced dissolution may offer a simpler, efficient and clean approach that does not require chemical additives thus significantly improves environmental benefits. Compared with the two current methods using ionic liquids and ultrasound, the underlying microscopic mechanism of the laser-induced dissolution approach is clear. The laser-excitation does not remarkably change the chemical mechanism of cellulose pretreatment and reactions, but the dissolution kinetics is remarkably accelerated as a result of resonance between the laser and cellulose vibrational modes, and therefore enhances the efficiency and economics of the biomass conversion process. We suggest that this method in combination with other methods such as ionic liquids could provide an efficient approach for cellulose dissolution at large-scale. We are currently performing mid-IR laser experiments to confirm our finding mechanisms so as to understand the dissolution of celluloses in combination with ionic liquids.

Acknowledgements This work has been supported by CNRS, the grant ANR-11-LABEX-0011-01, the National Science Foundation (NSF) USA via grants SI2-1148144 and 154941, the National Institutes of Health (NIH) USA via grants R01-GM079383 and R21- GM097617, and the IDRIS, CINES, TGCC centers for providing computer facilities (grants x2015077198, A0020710174 and A0030707721).

References

1. C.M. Payne, B.C. Knott, H.B. Mayes, H. Hansson, M.E. Himmel, M. Sandgren, J. Ståhlberg, G.T. Beckham, Fungal Cellulases, Chemical Reviews **115**(3), 1308 (2015). DOI 10.1021/cr500351c. URL http://dx.doi.org/10.1021/cr500351c
2. M.E. Himmel, S.Y. Ding, D.K. Johnson, W.S. Adney, M.R. Nimlos, J.W. Brady, T.D. Foust, Biomass recalcitrance: Engineering plants and enzymes for biofuels production, Science **315**(5813), 804 (2007). DOI 10.1126/science.1137016. URL http://science.sciencemag.org/content/315/5813/804
3. A. Aden, T. Foust, Technoeconomic analysis of the dilute sulfuric acid and enzymatic hydrolysis process for the conversion of corn stover to ethanol, Cellulose **16**(4), 535 (2009). DOI 10.1007/s10570-009-9327-8. URL http://dx.doi.org/10.1007/s10570-009-9327-8
4. Y. Nishiyama, P. Langan, H. Chanzy, Crystal structure and hydrogen bonding system in cellulose i(beta) from synchrotron x-ray and neutron fiber diffraction, J Am Chem Soc. **124**, 9074 (2002)
5. Y. Nishiyama, J. Sugiyama, H. Chanzy, P. Langan, Crystal structure and hydrogen bonding system in cellulose i(alpha) from synchrotron x-ray and neutron fiber diffraction, J Am Chem Soc. **125**, 14300 (2003)
6. B. Medronho, B. Lindman, Competing forces during cellulose dissolution: From solvents to mechanisms, Current Opinion in Colloid & Interface Science **19**(1), 32 (2014). DOI https://doi.org/10.1016/j.cocis.2013.12.001. URL http://www.sciencedirect.com/science/article/pii/S1359029413001350
7. J.F. Matthews, C.E. Skopec, P.E. Mason, P. Zuccato, R.W. Torget, J. Sugiyama, M.E. Himmel, J.W. Brady, Computer simulation studies of microcrystalline cellulose i, Carbohydrate Research **341**(1), 138 (2006). DOI http://dx.doi.org/10.1016/j.carres.2005.09.028
8. Y. Nishiyama, P. Langan, H. Chanzy, Crystal structure and hydrogen-bonding system in cellulose i from synchrotron x-ray and neutron fiber diffraction, Journal of the American Chemical Society **124**(31), 9074 (2002). DOI 10.1021/ja0257319
9. S.E. Levine, J.M. Fox, H.W. Blanch, D.S. Clark, A mechanistic model of the enzymatic hydrolysis of cellulose, Biotechnology and Bioengineering **107**(1), 37 (2010). DOI 10.1002/bit.22789. URL http://dx.doi.org/10.1002/bit.22789
10. A.C. Warden, B.A. Little, V.S. Haritos, A cellular automaton model of crystalline cellulose hydrolysis by cellulases, Biotechnology for Biofuels **4**(1), 1 (2011). DOI 10.1186/1754-6834-4-39
11. R.P. Swatloski, S.K. Spear, J.D. Holbrey, R.D. Rogers, Dissolution of cellose with ionic liquids, Journal of the American Chemical Society **124**(18), 4974 (2002). DOI 10.1021/ja025790m
12. K.M. Gupta, J. Jiang, Cellulose dissolution and regeneration in ionic liquids: A computational perspective, Chemical Engineering Science **121**, 180 (2015). DOI http://dx.doi.org/10.1016/j.ces.2014.07.025. 2013 Danckwerts Special Issue on Molecular Modelling in Chemical Engineering
13. H. Wang, G. Gurau, R.D. Rogers, Ionic liquid processing of cellulose, Chem. Soc. Rev. **41**, 1519 (2012). DOI 10.1039/C2CS15311D
14. J.P. Mikkola, A. Kirilin, J.C. Tuuf, A. Pranovich, B. Holmbom, L.M. Kustov, D.Y. Murzin, T. Salmi, Ultrasound enhancement of cellulose processing in ionic liquids: from dissolution towards functionalization, Green Chem. **9**, 1229 (2007)
15. A. Pinkert, K.N. Marsh, S. Pang, M.P. Staiger, Ionic liquids and their interaction with cellulose, Chem Rev. **109**, 6712 (2009)
16. H. Wang, G. Gurau, R.D. Rogers, Ionic liquid processing of cellulose, Chem. Soc. Rev. **41**, 15191537 (2012)
17. J. Luo, Z. Fang, R.L. Smith Jr., Ultrasound-enhanced conversion of biomass to biofuels, Progress in Energy and Combustion Science **41**, 56 (2013)
18. T. Kawasaki, J. Fujioka, T. Imai, K. Tsukiyama, Effect of mid-infrared free-electron laser irradiation on refolding of amyloid-like fibrils of lysozyme into native form., The protein journal **31**(8), 710 (2012). URL http://view.ncbi.nlm.nih.gov/pubmed/23054332

19. T. Kawasaki, J. Fujioka, T. Imai, K. Torigoe, K. Tsukiyama, Mid-infrared free-electron laser tuned to the amide I band for converting insoluble amyloid-like protein fibrils into the soluble monomeric form **29**(5), 1701 (2014). DOI 10.1007/s10103-014-1577-5. URL http://dx.doi.org/10.1007/s10103-014-1577-5
20. T. Kawasaki, T. Imai, K. Tsukiyama, Use of a Mid-Infrared Free-Electron Laser (MIR-FEL) for Dissociation of the Amyloid Fibril Aggregates of a Peptide, Journal of Analytical Sciences, Methods and Instrumentation **04**(01), 9 (2014). DOI 10.4236/jasmi.2014.41002. URL http://dx.doi.org/10.4236/jasmi.2014.41002
21. T. Kawasaki, T. Yaji, T. Imai, T. Ohta, K. Tsukiyama, Synchrotron-infrared microscopy analysis of amyloid fibrils irradiated by mid-infrared free-electron laser, American Journal of Analytical Chemistry **05**(06), 384 (2014). DOI 10.4236/ajac.2014.56047. URL http://dx.doi.org/10.4236/ajac.2014.56047
22. T. Kawasaki, T. Yaji, T. Ohta, K. Tsukiyama, IUCr, Application of mid-infrared free-electron laser tuned to amide bands for dissociation of aggregate structure of protein, Journal of Synchrotron Radiation **23**(1), 152 (2016). DOI 10.1107/yi5014. URL http://dx.doi.org/10.1107/yi5014
23. T.C. Gomes, M.S. Skaf, Cellulose-builder: a toolkit for building crystalline structures of cellulose, J Comput Chem. **33**, 1338 (2012)
24. D.J. Cosgrove, Re-constructing our models of cellulose and primary cell wall assembly, Current Opinion in Plant Biology **22**, 122 (2014). DOI https://doi.org/10.1016/j.pbi.2014.11.001. URL http://www.sciencedirect.com/science/article/pii/S1369526614001538. SI: Cell biology
25. S.Y. Ding, M.E. Himmel, The maize primary cell wall microfibril: a new model derived from direct visualization, J. Agric. Food Chem. **54**, 597 (2006)
26. K. Mazeau, Structural micro-heterogeneities of crystalline iβ-cellulose, Cellulose **12**, 339 (2005)
27. J.F. Matthews, C.E. Skopec, P. Mason, P. Zuccato, R. Torget, J. Sugiyama, M. Himmel, J. Brady, Computer simulation studies of microcrystalline cellulose iβ, Carbohydr Res. **341**, 138 (2006)
28. M. Bergenstrahle, L. Berglund, K. Mazeau, Thermal response in crystalline i cellulose: a molecular dynamics study, J Phys Chem B **111**, 9138 (2007)
29. A.S. Gross, J.W. Chu, On the molecular origins of biomass recalcitrance: the interaction network and solvation structures of cellulose microfibrils, J Phys Chem B **114**, 1333 (2010)
30. A.S. Gross, A.T. Bell, J.W. Chu, Thermodynamics of cellulose solvation in water and the ionic liquid 1-butyl-3-methylimidazolim chloride, The Journal of Physical Chemistry B **115**(46), 13433 (2011). DOI 10.1021/jp202415v. URL https://doi.org/10.1021/jp202415v. PMID: 21950594
31. Q. Zhang, V. Bulone, H. Agren, Y. Tu, A molecular dynamics study of the thermal response of crystalline cellulose iβ, Cellulose **18**, 207 (2011)
32. J.F. Matthews, M.E. Himmel, M.F. Crowley, Conversion of cellulose iα to iβ via a high temperature intermediate (i-ht) and other cellulose phase transformations, Cellulose **19**, 297 (2011)
33. J.F. Matthews, M. Bergenstrahle, G.T. Beckham, M.E. Himmel, M.R. Nimlos, J.W. Brady, M.F. Crowley, High-temperature behavior of cellulose i, J Phys Chem B **115**, 2155 (2011)
34. J.F. Matthews, G.T. Beckham, M. Bergenstrahle-Wohlert, J.W. Brady, M.E. Himmel, M.F. Crowley, Comparison of cellulose iβ simulations with three carbohydrate force fields, J Chem Theory Comput **8**, 735 (2012)
35. P. Chen, Y. Nishiyama, J.L. Putaux, K. Mazeau, Diversity of potential hydrogen bonds in cellulose i revealed by molecular dynamics simulation, Cellulose **21**, 897 (2014)
36. D.P. Oehme, M.T. Downton, M.S. Doblin, J. Wagner, M.J. Gidley, A. Bacic, Unique aspects of the structure and dynamics of elementary iβ cellulose microfibrils revealed by computational simulations, Plant Physiol. **168**, 3 (2015)
37. O. Guvench, S.N. Greene, G. Kamath, J.W. Brady, R.M. Venable, R.W. Pastor, A.D.J. Mackerell, Additive empirical force field for hexopyranose monosaccharides., J Comput Chem. **29**, 2543 (2008)

38. O. Guvench, E.R. Hatcher, R.M. Venable, R.W. Pastor, A.J. Mackerell, Charmm additive all-atom force field for glycosidic linkages between hexopyranoses, J Chem Theory Comput. **5**, 2353 (2009)
39. W.L. Jorgensen, J. Chandrasekhar, J.D. Madura, R.W. Impey, M.L. Klein, Comparison of simple potential functions for simulating liquid water, J. Chem. Phys. **79**, 926 (1983)
40. E. Lindahl, B. Hess, D. van der Spoel, Gromacs 3.0: A package for molecular simulation and trajectory analysis, J. Mol. Mod. **7**, 306 (2001)
41. J.P. Ryckaert, G. Cicotti, H.J.C. Berendsen, Numerical integration of the cartesian equations of motion of a system with constraints: Molecular dynamics of n-alkanes, J. Com. Phys. **23**, 327 (1977)
42. T. Darden, D. York, L. Pedersen, Particle mesh Ewald: An Nlog(N) method for Ewald sums in large systems., J. Chem. Phys. **98**, 10089 (1993)
43. H.J.C. Berendsen, J.P.M. Postma, W.F. van Gunsteren, A. Dinola, J.R. Haak, Molecular-dynamics with coupling to an external bath, J. Chem. Phys. **81**, 3684 (1984)
44. N.T. Van-Oanh, C. Falvo, F. Calvo, D. Lauvergnat, M. Basire, M.P. Gaigeot, P. Parneix, Improving anharmonic infrared spectra using semiclassically prepared molecular dynamics simulations, Phys. Chem. Chem. Phys. **14**(7), 2381 (2012). DOI 10.1039/c2cp23101h. URL http://dx.doi.org/10.1039/c2cp23101h
45. M.H. Viet, P. Derreumaux, M.S. Li, C. Roland, C. Sagui, P.H. Nguyen, Picosecond dissociation of amyloid fibrils with infrared laser: a nonequilibrium simulation study, J. Chem. Phys. **143**, 155101 (2015)
46. M.H. Viet, P.M. Truong, P. Derreumaux, M.S. Li, C. Roland, C. Sagui, P.H. Nguyen, Picosecond melting of peptide nanotubes using an infrared laser: a nonequilibrium simulation study, Phys. Chem. Chem. Phys **17**, 27275 (2015)
47. V.H. Man, F. Pan, C. Sagui, C. Roland, Comparative melting and healing of B-DNA and Z-DNA by an infrared laser pulse, The Journal of Chemical Physics **144**(14), 145101+ (2016). DOI 10.1063/1.4945340. URL http://dx.doi.org/10.1063/1.4945340
48. V.H. Man, N.T. Van-Oanh, P. Derreumaux, M.S. Li, C. Roland, C. Sagui, P.H. Nguyen, Picosecond infrared laser-induced all-atom nonequilibrium molecular dynamics simulation of dissociation of viruses, Phys. Chem. Chem. Phys. (2016). DOI 10.1039/c5cp07711g. URL http://dx.doi.org/10.1039/c5cp07711g
49. M. Tsuboi, Infrared spectrum and crystal structure of cellulose, Journal of Polymer Science **25**(109), 159 (1957). DOI 10.1002/pol.1957.1202510904. URL https://onlinelibrary.wiley.com/doi/abs/10.1002/pol.1957.1202510904
50. H. Higgins, C. Stewart, K. Harrington, Infrared spectra of cellulose and related polysaccharides, Journal of Polymer Science **51**(155), 59 (1961). DOI 10.1002/pol.1961.1205115505. URL https://onlinelibrary.wiley.com/doi/abs/10.1002/pol.1961.1205115505
51. T. Kondo, The assignment of ir absorption bands due to free hydroxyl groups in cellulose, Cellulose **4**(4), 281 (1997). DOI 10.1023/A:1018448109214. URL https://doi.org/10.1023/A:1018448109214
52. Y. Marechal, H. Chanzy, The hydrogen bond network in iβ cellulose as observed by infrared spectrometry, J. Mo. Phys. **523**, 183 (2000)
53. M. Nelson, R.T. O'Connor, Relation of certain infrared bands to cellulose crystallinity and crystal latticed type. part i. spectra of lattice types i, ii, iii and of amorphous cellulose, Journal of Applied Polymer Science **8**(3), 1311 (1964). DOI 10.1002/app.1964.070080322. URL https://onlinelibrary.wiley.com/doi/abs/10.1002/app.1964.070080322
54. M. Nelson, R.T. O'Connor, Relation of certain infrared bands to cellulose crystallinity and crystal latticed type. part ii. a new infrared ratio for estimation of crystallinity in celluloses i and ii, Journal of Applied Polymer Science **8**(3), 1325 (1964). DOI 10.1002/app.1964.070080323. URL https://onlinelibrary.wiley.com/doi/abs/10.1002/app.1964.070080323
55. J. Max, C. Chapados, Isotope effects in liquid water by infrared spectroscopy. iii. h2o and d2o spectra from 6000to0cm1, The Journal of Chemical Physics **131**(18), 184505 (2009). DOI 10.1063/1.3258646. URL https://doi.org/10.1063/1.3258646

56. Y. Marechal, The molecular structure of liquid water delivered by absorption spectroscopy in the whole ir region completed with thermodynamics data, Journal of Molecular Structure **1004**(1), 146 (2011). DOI https://doi.org/10.1016/j.molstruc.2011.07.054. URL http://www.sciencedirect.com/science/article/pii/S0022286011006247
57. V. Agarwal, G.W. Huber, W.C. Conner, S.M. Auerbach, Simulating infrared spectra and hydrogen bonding in cellulose iβ at elevated temperatures, The Journal of Chemical Physics **135**(13), 134506 (2011). DOI 10.1063/1.3646306. URL https://doi.org/10.1063/1.3646306
58. W.L. Jorgensen, J. Chandrasekhar, J.D. Madura, R.W. Impey, M.L. Klein, Comparison of simple potential functions for simulating liquid water, J. Chem. Phys. **79**, 926 (1983)
59. H.J.C. Berendsen, J.P.M. Postma, W.F. van Gunsteren, J. Hermans, *Intermolecular Forces* (Reidel, Dordrecht, 1981)
60. T. Kawasaki, J. Fujioka, T. Imai, K. Tsukiyama, Effect of mid-infrared free-electron laser irradiation on refolding of amyloid-like fibrils of lysozyme into native form, The Protein Journal **31**, 710 (2012)
61. T. Kawasaki, J. Fujioka, T. Imai, K. Torigoe, K. Tsukiyama, Mid-infrared free-electron laser tuned to the amide i band for converting insoluble amyloid-like protein fibrils into the soluble monomeric form, Lasers in Medical Science **29**, 1701 (2014)
62. T. Kawasaki, T. Imai, K. Tsukiyama, Use of a mid-infrared free-electron laser (mirfel) for dissociation of the amyloid fibril aggregates of a peptide, Journal of Analytical Sciences, Methods and Instrumentation **4**, 9 (2014)
63. T. Kawasaki, T. Yaji, T. Imai, T. Ohta, K. Tsukiyama, Synchrotron-infrared microscopy analysis of amyloid fibrils irradiated by mid-infrared free- electron laser, American Journal of Analytical Chemistry **5**, 384 (2014)
64. R. Marchessault, C. Liang, Infrared spectra of crystalline polysaccharides. iii. mercerized cellulose, Journal of Polymer Science **43**(141), 71 (1960). DOI 10.1002/pol.1960.1204314107. URL https://onlinelibrary.wiley.com/doi/abs/10.1002/pol.1960.1204314107
65. Y. Hishikawa, E. Togawa, T. Kondo, Characterization of individual hydrogen bonds in crystalline regenerated cellulose using resolved polarized ftir spectra, ACS Omega **2**(4), 1469 (2017). DOI 10.1021/acsomega.6b00364. URL https://doi.org/10.1021/acsomega.6b00364
66. B.D. Rabideau, A. Agarwal, A.E. Ismail, Observed mechanism for the breakup of small bundles of cellulose iα and iβ in ionic liquids from molecular dynamics simulations, J. Phys. Chem. B **117**, 3469 (2013)
67. H.M. Cho, A.S. Gross, J. Chu, Dissecting force interactions in cellulose deconstruction reveals the required solvent versatility for overcoming biomass recalcitrance, J. Am. Chem. Soc. **133**, 14033 (2011)
68. B. Lindman, G. Karlstrom, L. Stigsson, On the mechanism of dissolution of cellulose, J. Mol. Liq. **156**, 76 (2010)
69. P. Langan, Y. Nishiyama, H. Chanzy, A revised structure and hydrogen-bonding system in cellulose ii from a neutron fiber diffraction analysis, Journal of the American Chemical Society **121**(43), 9940 (1999). DOI 10.1021/ja9916254. URL https://doi.org/10.1021/ja9916254
70. P. Langan, Y. Nishiyama, H. Chanzy, X-ray structure of mercerized cellulose ii at 1 resolution, Biomacromolecules **2**(2), 410 (2001). DOI 10.1021/bm005612q. URL https://doi.org/10.1021/bm005612q. PMID: 11749200
71. H. Jisuke, S. Akinori, O. Junji, W. Sadayoshi, The confirmation of existences of cellulose iiii, iiiii, ivi, and ivii by the x-ray method, Journal of Polymer Science: Polymer Letters Edition **13**(1), 23 (1975). DOI 10.1002/pol.1975.130130104. URL https://onlinelibrary.wiley.com/doi/abs/10.1002/pol.1975.130130104
72. S.P.S. Chundawat, G. Bellesia, N. Uppugundla, L. da Costa Sousa, D. Gao, A.M. Cheh, U.P. Agarwal, C.M. Bianchetti, G.N. Phillips, P. Langan, V. Balan, S. Gnanakaran, B.E. Dale, Restructuring the crystalline cellulose hydrogen bond network enhances its depolymerization rate, Journal of the American Chemical Society **133**(29), 11163 (2011). DOI 10.1021/ja2011115. URL https://doi.org/10.1021/ja2011115. PMID: 21661764
73. Y.H.P. Zhang, J. Cui, L.R. Lynd, L.R. Kuang, A transition from cellulose swelling to cellulose dissolution by o-phosphoric acid: evidence from enzymatic hydroly-

sis and supramolecular structure, Biomacromolecules **7**(2), 644 (2006). DOI 10.1021/bm050799c. URL https://doi.org/10.1021/bm050799c. PMID: 16471942
74. A. Mittal, R. Katahira, M.E. Himmel, D.K. Johnson, Effects of alkaline or liquid-ammonia treatment on crystalline cellulose: changes in crystalline structure and effects on enzymatic digestibility, Biotechnology for Biofuels **4**(1), 41 (2011). DOI 10.1186/1754-6834-4-41. URL https://doi.org/10.1186/1754-6834-4-41
75. L. Zhong, J.F. Matthews, P.I. Hansen, M.F. Crowley, J.M. Cleary, R.C. Walker, M.R. Nimlos, C. Brooks III, W.S. Adney, M.E. Himmel, J.W. Brady, Computational simulations of the trchoderma reesei cellobiohydrolase i acting on microcrystalline cellulose iβ: The enzyme-substrate complex, Carbohydr. Res. **344**, 1984 (2009)
76. J. Wohlert, L.A. Berglund, A coarse-grained model for molecular dynamics simulations of native cellulose, J. Chem. Theory Comput. **7**, 753 (2011)
77. D.C. Glass, K. Moritsugu, X. Cheng, J.C. Smith, Reach coarse-grained simulation of a cellulose fiber, Biomacromolecules **13**, 2634 (2012)
78. G. Srinivas, X. Cheng, J.C. Smith, Coarse-grain model for natural cellulose fibrils in explicit water, J. Phys. Chem. B **118**, 3026 (2014)
79. A.B. Poma, M. Chwastyk, M.Cieplak, Coarse-grained model of the native cellulose iαi and the transformation pathways to the iβ allomorph, Cellulose **23**, 1573 (2016)